Unconventional Sequence of Fractional Quantum Hall States in Suspended Graphene

Benjamin E. Feldman,[1] Benjamin Krauss,[2] Jurgen H. Smet,[2] Amir Yacoby[1]*

Graphene provides a rich platform to study many-body effects, owing to its massless chiral charge carriers and the fourfold degeneracy arising from their spin and valley degrees of freedom. We use a scanning single-electron transistor to measure the local electronic compressibility of suspended graphene, and we observed an unusual pattern of incompressible fractional quantum Hall states that follows the standard composite fermion sequence between filling factors $\nu = 0$ and 1 but involves only even-numerator fractions between $\nu = 1$ and 2. We further investigated this surprising hierarchy by extracting the corresponding energy gaps as a function of the magnetic field. The sequence and relative strengths of the fractional quantum Hall states provide insight into the interplay between electronic correlations and the inherent symmetries of graphene.

Application of a strong perpendicular magnetic field B to a two-dimensional electron gas (2DEG) gives rise to flat energy bands called Landau levels (LLs), which normally contain a total of eB/h states, where e is the electron charge and h is Planck's constant. In graphene, each of these states has an additional fourfold degeneracy resulting from the spin and valley degrees of freedom, and the LLs possess an approximate SU(4) symmetry (*1*). Incompressible quantum Hall states are formed when the Fermi energy lies between LLs. In graphene, LLs are filled at filling factors $\nu = nh/eB = 4(N + 1/2)$ in the absence of electron-electron interactions (*2*–*4*), where n is the charge-carrier density and N is the orbital index. In this expression, the quantum Hall sequence is shifted by a half-integer, a distinctive signature that reflects the sublattice pseudospin of graphene.

When disorder is low and at high magnetic fields, Coulomb forces between electrons become important, and many-body effects emerge. One example is the fractional quantum Hall effect (FQHE), in which correlations between electrons generate excitations with fractional charge at certain rational filling fractions (*5*–*8*). Recently, the FQHE of Dirac fermions has attracted considerable attention (*9*–*22*). In graphene, the low dielectric constant and unusual band structure lead to FQH states with energy gaps that are larger than in GaAs at the same field, particularly in the $N = 1$ LL (*10*, *15*, *16*). Moreover, the SU(4) symmetry of charge carriers in graphene could yield FQH states without analogs in GaAs (*11*, *12*, *19*). The FQHE was recently observed (*23*–*25*) in suspended graphene samples at $\nu = 1/3$ and 2/3, and transconductance fluctuations also showed evidence of a state at $\nu = 2/5$ (*26*). Measurements of graphene on hexagonal boron nitride substrates (*27*) revealed further FQH states at all multiples of $\nu = 1/3$ up to 13/3, except at $\nu = 5/3$. The absence of a FQH state at $\nu = 5/3$ might result from low-lying excitations associated with SU(2) or SU(4) symmetry, but alternate scenarios associated with disorder could not be ruled out in earlier studies (*27*).

Here, we report local electronic compressibility measurements of a suspended graphene flake performed with a scanning single-electron transistor (SET) (Fig. 1A) (*28*, *29*). By modulating the carrier density and monitoring the resulting change in SET current, we measure both the local chemical potential μ and the local inverse electronic compressibility of the graphene flake (inverse compressibility $\kappa^{-1} = n^2 d\mu/dn$, but hereafter we drop the prefactor and use the term to mean $d\mu/dn$). Therefore, our local technique provides a direct thermodynamic measurement of bulk sample properties and is sensitive to weak effects that may be obscured by disorder in global transport studies.

The inverse compressibility as a function of carrier density and magnetic field is shown in Fig. 1B. At zero magnetic field, we observe an incompressible peak that arises from the vanishing density of states at the charge neutrality point in graphene. For $B > 0$, strong incompressible behavior occurs at $\nu = 4(N + 1/2)$, confirming the monolayer nature of our sample. In addition to the expected single-particle quantum Hall features, we observe incompressible states at intermediate integer filling factors $\nu = 0$, 1, 3, 4, 5, 7, 8, and 9. These integer broken-symmetry states arise from interactions among electrons (*25*, *27*, *30*, *31*) and are visible at fields well below 1 T, indicating the high quality of our sample. Most intriguing, however, is the appearance of incompressible peaks at fractional filling factors, the strongest of which emerge around $B = 1$ T. It is straightforward to distinguish FQH states from oscillations in compressibility caused by localized states. Localized states occur at a constant density offset from their parent quantum Hall state and are therefore parallel to lines of constant filling factor in the nB plane (*4*). When inverse compressibility is plotted as a function of filling factor (Fig. 1C), localized states curve as the magnetic field is changed, whereas any incompressible behavior caused by an integer or FQH state appears as a vertical feature (*32*).

Figure 2A shows a finer measurement of the inverse compressibility as a function of filling factor and magnetic field for $\nu < 1$. Incompressible peaks occur at $\nu = 1/3$, 2/3, 2/5, 3/5, 3/7, 4/7, and 4/9, reproducing the standard composite fermion sequence observed in GaAs. We resolve the strongest incompressible states, $\nu = 1/3$ and 2/3, down to $B \approx 1$ T, although $\nu = 2/3$ weakens considerably below 4 T. As the filling factor denominator increases, the field at which the corresponding state emerges also increases, with $\nu = 4/9$ only apparent above $B \approx 9$ T.

Between $\nu = 1$ and 2, we observe a different pattern of incompressible behavior (Fig. 2B). Surprisingly, no FQH states with odd numerators occur in this regime. Instead, the system condenses into incompressible states only at $\nu = 4/3$, 8/5, 10/7, and 14/9. The incompressible peaks at $\nu = 4/3$ and 8/5 are the most robust, persisting down to ~1 and ~1.5 T, respectively. In graphene, $\nu = 2$ corresponds to a filled LL ($N = 0$), so it is natural to label FQH states with the filling fraction $\nu^* = 2 - \nu$. Doing so reveals a clear pattern of incompressible peaks at $\nu^* = 2p/(4p \pm 1)$ for $p \leq 2$, which is similar to the composite fermion sequence, except that only filling fractions with even numerators lead to incompressible states.

The absence of odd-numerator fractions indicates that a robust underlying symmetry enables low-lying excitations, preventing the formation of incompressible states. One possible explanation is that the Zeeman effect lifts spin degeneracy, but valley symmetry remains intact, allowing large valley skyrmions to form with a minimal energy penalty at odd-numerator filling factors. The behavior we observe between $\nu = 1$ and 2 is reminiscent of results from strained Si and AlAs 2DEGs, which also have a valley degree of freedom and exhibit weakened odd-numerator states (*33*–*36*). However, the analogy is not perfect. The large effective mass and g-factor in these semiconducting materials lead to fully spin-polarized LLs due to single-particle effects; in contrast, the Zeeman energy is substantially smaller than the LL separation in graphene. In valley-symmetric AlAs, the energy gap at $\nu = 1/3$ is large compared with that at $\nu = 5/3$ (*35*), opposite from the behavior we observe at $\nu^* = 1/3$ and 5/3 when we account for the half-integer shift of LLs in graphene. This suggests that the total electron density, and not just the filling fraction, may play an important role in electronic interactions in the lowest LL, a

[1]Department of Physics, Harvard University, Cambridge, MA 02138, USA. [2]Max-Planck-Institut für Festkörperforschung, Heisenbergstrasse 1, D-70569 Stuttgart, Germany.

*To whom correspondence should be addressed. E-mail: yacoby@physics.harvard.edu

topic that has only recently been explored (*37*). Moreover, whereas the incompressible behavior we observe between ν = 1 and 2 is consistent with SU(2) symmetry, it is evident that this symmetry does not persist between ν = 0 and 1, where the full composite fermion sequence is present. The differing behavior above and below ν = 1 suggests an intriguing interplay between the inherent symmetries of graphene and electronic correlations in the lowest LL. This is different from strained Si, in which odd-numerator states are weakened both above and below ν = 1 (*33*). In the valley-symmetric AlAs data from (*35*), both ν = 7/5 and 3/5 states are absent, whereas ν = 8/5 and 2/5 are visible. At higher magnetic fields, however, the ν = 3/5 state is apparent (*37*), similar to the behavior in graphene.

Averaging over a range of magnetic fields helps to reduce fluctuations from localized states because they do not occur at constant filling factor as the magnetic field is varied. Figure 2C shows the inverse compressibility between ν = 0 and 1, averaged over 9 to 11.9 T (blue), and between ν = 1 and 2, averaged over 4.9 to 6.4 T (red). These curves reveal clear incompressible peaks centered at the filling fractions discussed above, as well as negative contributions to the inverse compressibility immediately surrounding each FQH state, which can be ascribed to interactions among the quasi-particles and quasi-holes involved in the FQHE (*38*). A slight incompressible peak occurring at ν = 1.65 (Fig. 2C) may indicate the emergence of a FQH state at ν = 5/3; however, it is much weaker than all other multiples of ν = 1/3 and is therefore consistent with the conclusion that all odd-numerator FQH states are suppressed for ν > 1.

Integrating the inverse compressibility with respect to carrier density allows us to extract the step in chemical potential $\Delta\mu_\nu$ associated with each FQH state and thereby determine the corresponding energy gap Δ_ν. Figure 3A displays the chemical potential as a function of carrier density at B = 11.9 T. We define $\Delta\mu_\nu$ as the difference between the local maximum and minimum in the chemical potential, and the values for each FQH state as a function of magnetic field are plotted in Fig. 3, B and C. We define the zero of $d\mu/dn$ based on its value at ν = 1/2 to accurately determine $\Delta\mu_\nu$ at each field (fig. S8) (*32*). Because the chemical potential is defined with respect to electrons, the step in chemical potential must be multiplied by the ratio of the quasi-particle charge to the electron charge to obtain the energy gap of fractionally charged quasi-particles.

The steps in chemical potential at each multiple of ν = 1/3 have comparable magnitudes (Fig. 3B), and they scale approximately linearly with the field. The linear dependence of the FQH energy gaps on the magnetic field is surprising because states driven by electronic interactions are expected to scale as $B^{1/2}$; the origin of this behavior is unclear. The steps in chemical potential at ν = 2/5, 3/5, and 8/5 are smaller and also depend approximately linearly on the magnetic field, although we cannot rule out a $B^{1/2}$ scaling. The steps in chemical potential at ν = 3/7, 4/7, 10/7,

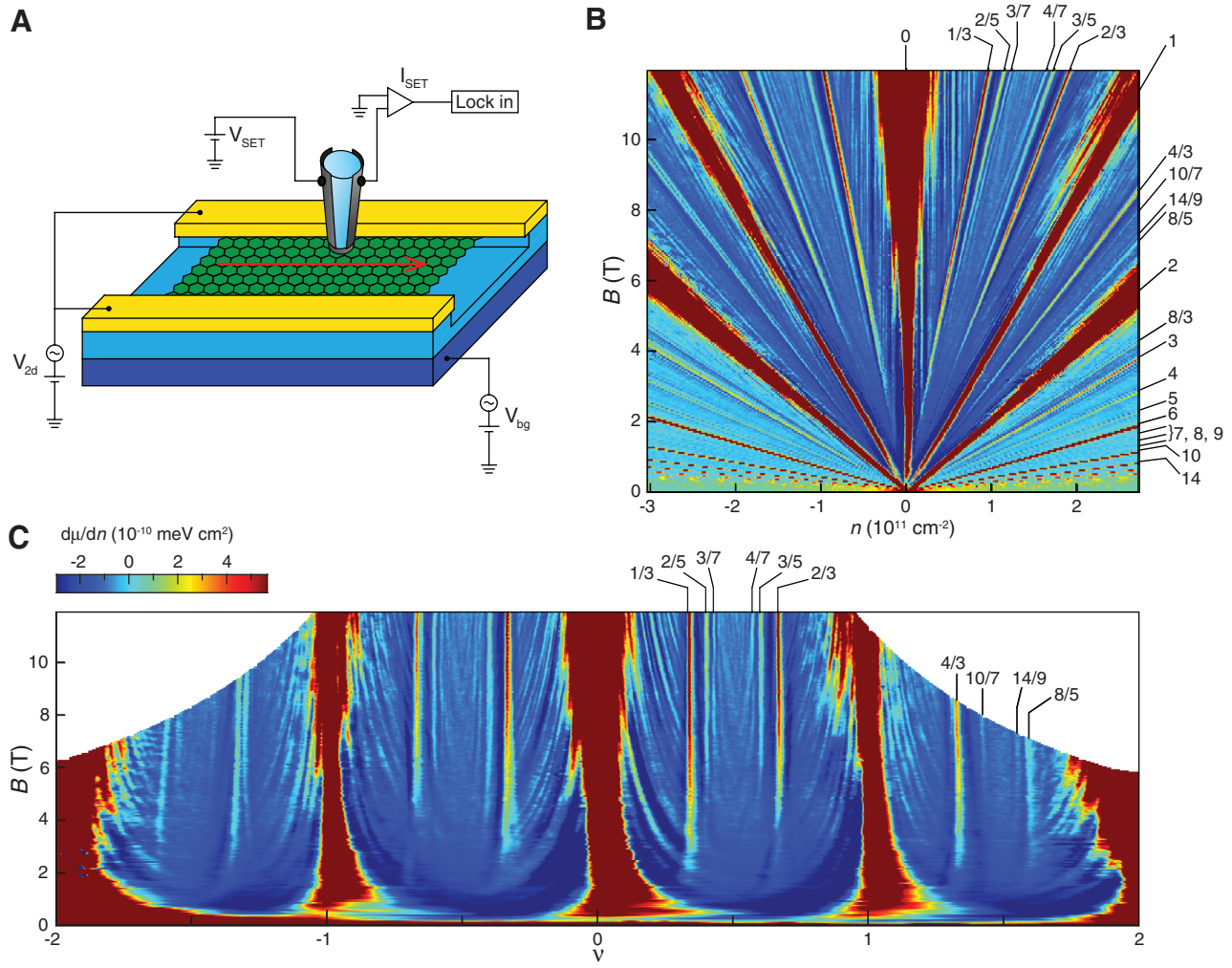

Fig. 1. Measurement setup and Landau fan. (**A**) The SET is ~100 nm in size and is held 50 to 150 nm above the graphene flake. The red arrow indicates the path of the spatial scans in Fig. 4. V, voltage; I, current. (**B**) Inverse compressibility $d\mu/dn$ as a function of carrier density n and magnetic field B. (**C**) Data from (B) plotted as a function of filling factor ν. Vertical features correspond to quantum Hall states, whereas localized states curve as the magnetic field is changed. Principal integer and FQH states are labeled in (B) and (C). These panels share the same color scale.

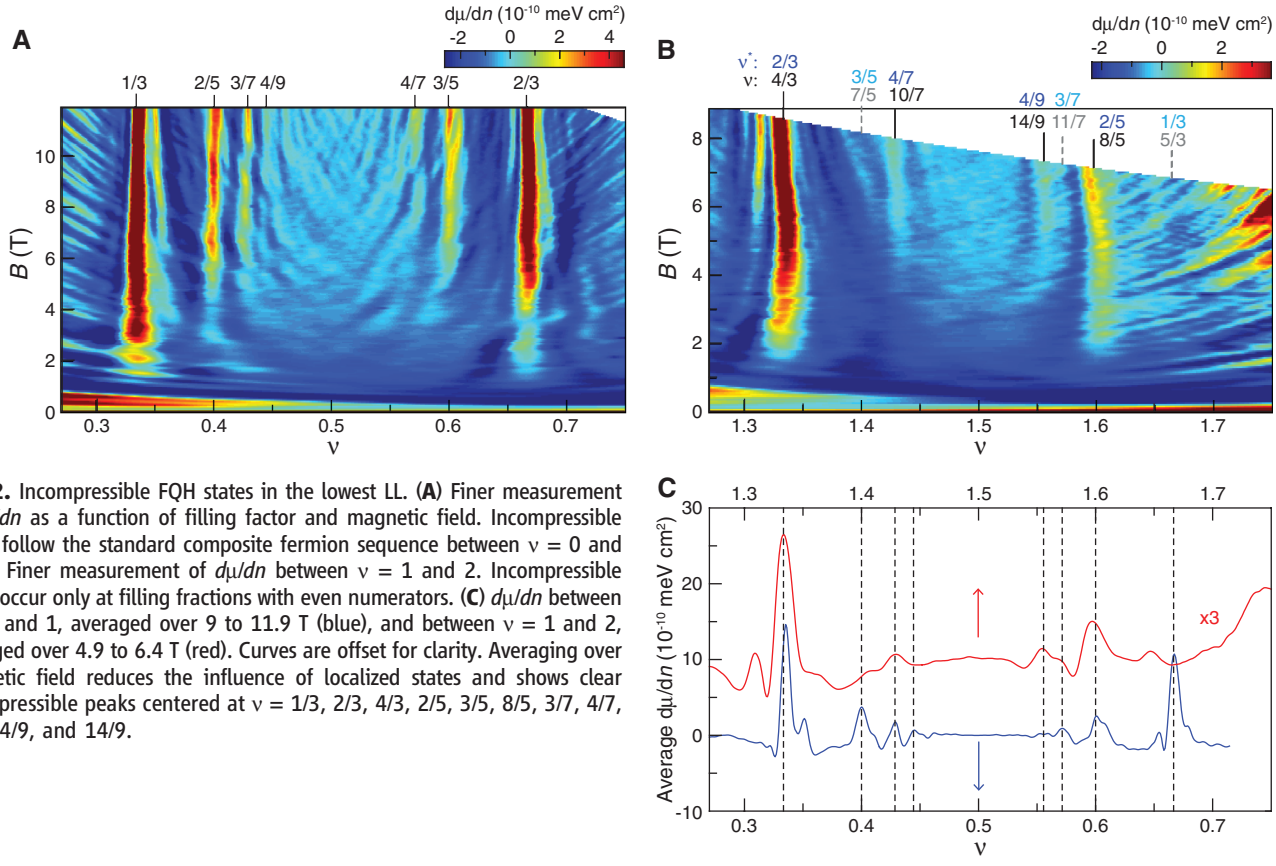

Fig. 2. Incompressible FQH states in the lowest LL. (**A**) Finer measurement of $d\mu/dn$ as a function of filling factor and magnetic field. Incompressible states follow the standard composite fermion sequence between $\nu = 0$ and 1. (**B**) Finer measurement of $d\mu/dn$ between $\nu = 1$ and 2. Incompressible states occur only at filling fractions with even numerators. (**C**) $d\mu/dn$ between $\nu = 0$ and 1, averaged over 9 to 11.9 T (blue), and between $\nu = 1$ and 2, averaged over 4.9 to 6.4 T (red). Curves are offset for clarity. Averaging over magnetic field reduces the influence of localized states and shows clear incompressible peaks centered at $\nu = 1/3$, 2/3, 4/3, 2/5, 3/5, 8/5, 3/7, 4/7, 10/7, 4/9, and 14/9.

4/9, and 14/9 are even smaller (Fig. 3C), and their extracted magnitudes fluctuate substantially as a function of the magnetic field, presumably because of localized states at the measurement point.

The energy gaps obtained from compressibility, which yield the cost of adding charged quasi-particle excitations to the system, have a slightly different physical meaning from those obtained in activation measurements, which probe the energy separation between the ground state and lowest excited state at a given filling factor. Nonetheless, the energy gaps that we extract (Fig. 3) are comparable to results from activation studies (*23*, *27*), which yielded $\Delta_{1/3} \approx$ 1.4 to 1.8 meV at 12 T and $\Delta_{4/3} \approx 1.4$ meV at 35 T. A comparison to $\Delta_{4/3}$ at 35 T is difficult because of the discrepancy in field strength; however, extrapolating the linear slope we measure in $\Delta_{4/3}$ yields a value of ~2.8 meV at 35 T. At the highest available magnetic fields, our measured energy gaps are only slightly smaller than theoretical predictions at $\nu = 1/3$ but are 3 to 10 times smaller than those theoretically predicted at $\nu = 2/3$, 4/3, 2/5, and 8/5 (table S1) (*9*, *10*, *12*, *15*, *16*, *21*, *32*). This discrepancy probably results in part from sample disorder, which smears out the cusps in $\mu(n)$ and, therefore, decreases the apparent step in chemical potential. The effects of disorder can be partially mitigated by linear extrapolation of the negative slope in $\mu(n)$ surrounding each fractional quantum Hall state (fig. S9) (*32*, *39*). The widths δn of the most

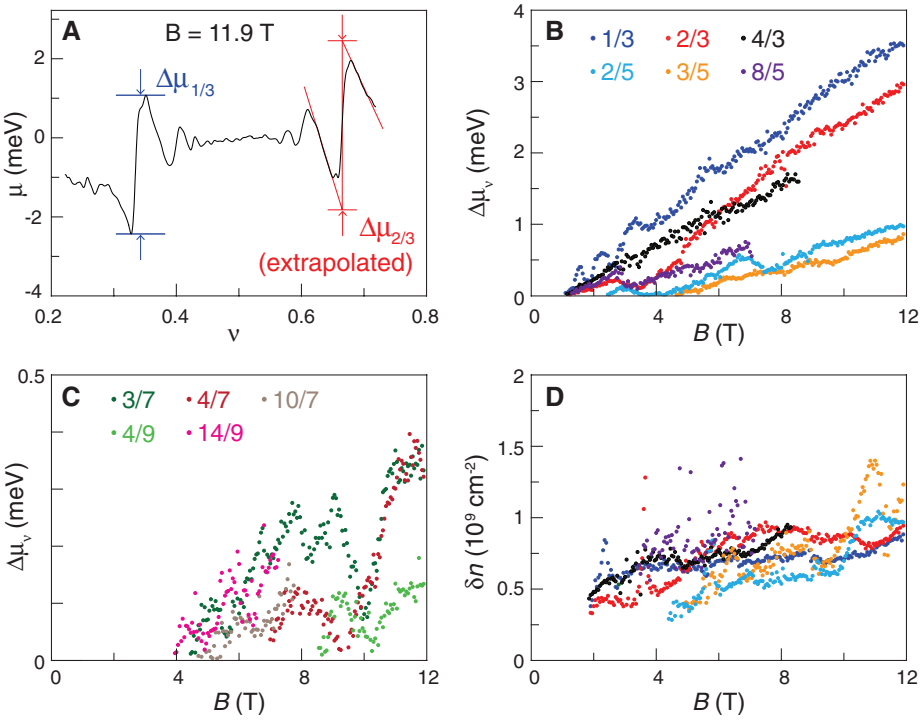

Fig. 3. Steps in chemical potential and incompressible peak widths. (**A**) Chemical potential relative to its value at $\nu = 1/2$ as a function of carrier density at 11.9 T. The step in chemical potential of each incompressible state is given by the difference in chemical potential between the local maximum and minimum (blue). Data presented in (B) and (C) were extracted using this method. (**B**) Steps in chemical potential associated with FQH states at measured multiples of $\nu = 1/3$ and 1/5 as a function of magnetic field. (**C**) Steps in chemical potential of FQH states at measured multiples of $\nu = 1/7$ and 1/9 as a function of magnetic field. (**D**) Incompressible peak width of the FQH states as a function of magnetic field. Colors are same as in (B).

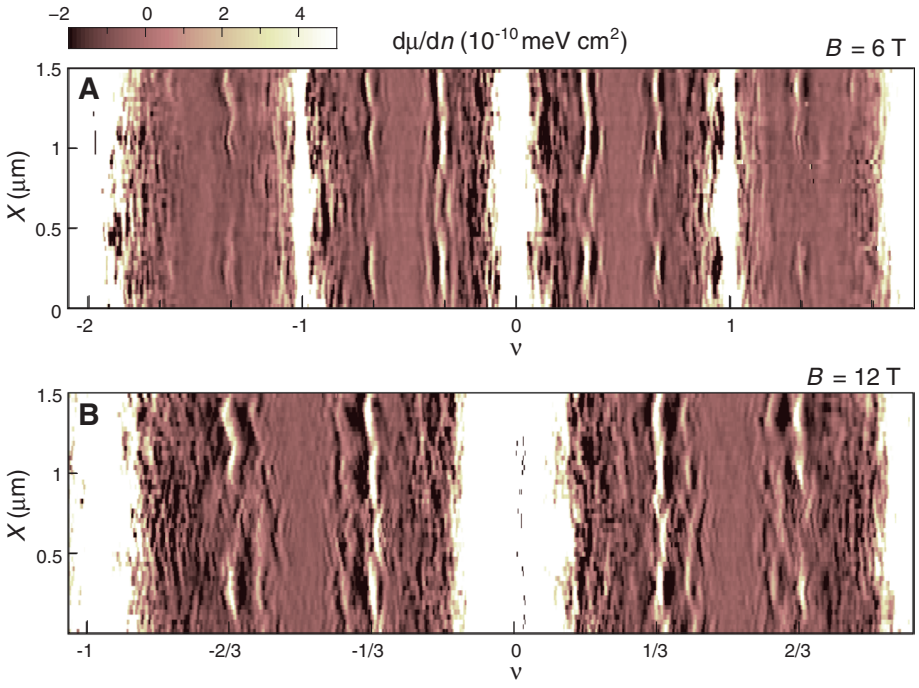

Fig. 4. Spatial dependence of FQH states. (**A**) $d\mu/dn$ as a function of filling factor and position X along the flake (red arrow in Fig. 1) at B = 6 T. (**B**) $d\mu/dn$ as a function of carrier density and position at B = 12 T. At both fields, we observe density fluctuations and variations in the strength of the FQH states as a function of position. States at ν = 2/3 and 4/3 appear more susceptible to disorder than does ν = 1/3.

robust FQH states (Fig. 3D) were determined by fitting a Gaussian to the incompressible peak at each filling factor. They are only weakly dependent on magnetic field, suggesting that δn reflects the amount of local disorder in our device (*4*). The exceptionally small peak widths provide another indication that the sample is especially clean.

Together, the unconventional sequence and relative strengths of the FQH states provide insight into the interplay between electronic interactions and symmetry in graphene. Between ν = 0 and 1, the compressibility is approximately symmetric about ν = 1/2, suggesting that the fourfold spin and valley degeneracy is fully lifted. In contrast, the missing odd-numerator states indicate that one symmetry persists between ν = 1 and 2. Nonetheless, the behavior in each regime exhibits some surprising similarities. Notably, the incompressible states that we observe above and below ν = 1 have comparable energy gaps. Further study is necessary to elucidate the exact spin and valley ordering of each state; for example, tilted field measurements decouple Zeeman splitting from orbital effects and could provide insight into spin polarization.

All of the measurements described above were taken at one position. Line scans of the inverse compressibility as a function of filling factor and position at B = 6 and 12 T are shown in Fig. 4, A and B, respectively. The gate voltages at which the incompressible peaks occur vary with position, which can be explained by local density fluctuations. The magnitude of these fluctuations is similar to the width of the FQH states and may explain why the FQHE has been so difficult to observe in transport studies: Different regions of the sample form a given FQH state at different back-gate voltages. Figure 4 also shows that incompressible peak magnitude fluctuates substantially as a function of position. Although some incompressible states, such as those at ν = 1/3, persist at virtually all positions, others are more susceptible to disorder. Both ν = 2/3 and 4/3 fully disappear in some locations, which seem to be correlated with the areas where the integer quantum Hall states are wider, a sign that local disorder is comparatively large. Despite the existence of disordered regions, the ability to perform local measurements reveals a multitude of FQH states in the cleanest areas. The observation of incompressible behavior at multiples of ν = 1/9 indicates a substantial improvement in sample quality; together with the unconventional pattern of FQH states, this shows that graphene provides an especially rich platform in which to investigate correlated electronic states and their interplay with underlying symmetry.

References and Notes

1. K. Nomura, A. H. MacDonald, *Phys. Rev. Lett.* **96**, 256602 (2006).
2. K. S. Novoselov *et al.*, *Nature* **438**, 197 (2005).
3. Y. B. Zhang, Y. W. Tan, H. L. Stormer, P. Kim, *Nature* **438**, 201 (2005).
4. J. Martin *et al.*, *Nat. Phys.* **5**, 669 (2009).
5. D. C. Tsui, H. L. Stormer, A. C. Gossard, *Phys. Rev. Lett.* **48**, 1559 (1982).
6. R. B. Laughlin, *Phys. Rev. Lett.* **50**, 1395 (1983).
7. J. K. Jain, *Phys. Rev. Lett.* **63**, 199 (1989).
8. B. I. Halperin, *Helv. Phys. Acta* **56**, 75 (1983).
9. V. M. Apalkov, T. Chakraborty, *Phys. Rev. Lett.* **97**, 126801 (2006).
10. C. Töke, P. E. Lammert, V. H. Crespi, J. K. Jain, *Phys. Rev. B* **74**, 235417 (2006).
11. M. O. Goerbig, N. Regnault, *Phys. Rev. B* **75**, 241405 (2007).
12. C. Töke, J. K. Jain, *Phys. Rev. B* **75**, 245440 (2007).
13. K. Yang, S. Das Sarma, A. H. MacDonald, *Phys. Rev. B* **74**, 075423 (2006).
14. D. V. Khveshchenko, *Phys. Rev. B* **75**, 153405 (2007).
15. N. Shibata, K. Nomura, *Phys. Rev. B* **77**, 235426 (2008).
16. N. Shibata, K. Nomura, *J. Phys. Soc. Jpn.* **78**, 104708 (2009).
17. Z. Papić, M. O. Goerbig, N. Regnault, *Solid State Commun.* **149**, 1056 (2009).
18. Z. Papić, M. O. Goerbig, N. Regnault, *Phys. Rev. Lett.* **105**, 176802 (2010).
19. S. Modak, S. S. Mandal, K. Sengupta, *Phys. Rev. B* **84**, 165118 (2011).
20. Z. Papić, D. A. Abanin, Y. Barlas, R. N. Bhatt, *Phys. Rev. B* **84**, 241306 (2011).
21. C. Tőke, J. K. Jain, *J. Phys. Condens. Matter* **24**, 235601 (2012).
22. M. O. Goerbig, N. Regnault, *Phys. Scr. T* **146**, 014017 (2012).
23. F. Ghahari, Y. Zhao, P. Cadden-Zimansky, K. Bolotin, P. Kim, *Phys. Rev. Lett.* **106**, 046801 (2011).
24. K. I. Bolotin, F. Ghahari, M. D. Shulman, H. L. Stormer, P. Kim, *Nature* **462**, 196 (2009).
25. X. Du, I. Skachko, F. Duerr, A. Luican, E. Y. Andrei, *Nature* **462**, 192 (2009).
26. D. S. Lee, V. Skákalová, R. T. Weitz, K. von Klitzing, J. H. Smet, *Phys. Rev. Lett.* **109**, 056602 (2012).
27. C. R. Dean *et al.*, *Nat. Phys.* **7**, 693 (2011).
28. M. J. Yoo *et al.*, *Science* **276**, 579 (1997).
29. A. Yacoby, H. F. Hess, T. A. Fulton, L. N. Pfeiffer, K. W. West, *Solid State Commun.* **111**, 1 (1999).
30. Y. Zhang *et al.*, *Phys. Rev. Lett.* **96**, 136806 (2006).
31. Z. Jiang, Y. Zhang, H. L. Stormer, P. Kim, *Phys. Rev. Lett.* **99**, 106802 (2007).
32. Supplementary materials are available on *Science* Online.
33. K. Lai *et al.*, *Phys. Rev. Lett.* **93**, 156805 (2004).
34. N. C. Bishop *et al.*, *Phys. Rev. Lett.* **98**, 266404 (2007).
35. M. Padmanabhan, T. Gokmen, M. Shayegan, *Phys. Rev. Lett.* **104**, 016805 (2010).
36. M. Padmanabhan, T. Gokmen, M. Shayegan, *Phys. Rev. B* **80**, 035423 (2009).
37. M. Padmanabhan, T. Gokmen, M. Shayegan, *Phys. Rev. B* **81**, 113301 (2010).
38. J. P. Eisenstein, L. N. Pfeiffer, K. W. West, *Phys. Rev. Lett.* **68**, 674 (1992).
39. V. S. Khrapai *et al.*, *Phys. Rev. Lett.* **100**, 196805 (2008).

Acknowledgments: We thank M. T. Allen for useful discussions and for helping to current anneal the device and B. I. Halperin, D. Abanin, J. K. Jain, S. das Sarma, J. Martin, V. Venkatachalam, S. Hart, and G. Ben-Shach for helpful discussions. This work is supported by the U.S. Department of Energy, Office of Basic Energy Sciences, Division of Materials Sciences and Engineering, under award no. DE-SC0001819. J.H.S. and B.K. acknowledge financial support from the Deutsche Forschungsgemeinschaft graphene priority program, and B.K. acknowledges financial support from the Bayer Science and Education Foundation. This work was performed in part at the Center for Nanoscale Systems (of Harvard Univ.), a member of the National Nanotechnology Infrastructure Network, which is supported by the NSF under award no. ECS-0335765.

Supplementary Materials

www.sciencemag.org/cgi/content/full/337/6099/1196/DC1
Materials and Methods
Supplementary Text
Figs. S1 to S10
Table S1
References (*40*–*43*)

16 May 2012; accepted 25 July 2012
10.1126/science.1224784